Available online at www.sciencedirect.com

jmr&t Journal of Materials Research and Technology

journal homepage: www.elsevier.com/locate/jmrt

Effects of natural aging on the artificial aging kinetics and responses of Al–5Mg–3Zn–1Cu (wt.%) alloy

Chuan Lei [a], *Nannan Zhang* [a], *Qudong Wang* [a,*], *Mahmoud Ebrahimi* [a], *Dezhi Li* [b], *Huaping Tang* [c], *Huisheng Cai* [a]

[a] *National Engineering Research Center of Light Alloy Net Forming and State Key Laboratory of Metal Matrix Composites, School of Materials Science and Engineering, Shanghai Jiao Tong University, Shanghai 200240, China*
[b] *Warwick Manufacturing Group, University of Warwick, Coventry CV4 7AL, UK*
[c] *Ji Hua Laboratory, Foshan, Guangdong, 528255, China*

ARTICLE INFO

Article history:
Received 1 May 2023
Accepted 14 July 2023
Available online 17 July 2023

Keywords:
Al–5Mg–3Zn–1Cu alloy
Natural aging
Artificial aging
Precipitation mechanisms
Precipitate-free zone

ABSTRACT

Effects of natural aging (NA) on artificial aging (AA) behavior of Al–5Mg–3Zn–1Cu alloy were studied from the perspectives of kinetics and microstructure evolution. The results show that short-term NA (24 h) has marginal effects on AA at any temperature, as well as long-term NA (>240 h) on low-temperature AA (120 °C), but long-term NA can accelerate aging kinetics and alleviate severe hardening ability attenuation at high temperatures (>150 °C). Analysis of the precipitates evolution demonstrates that such attenuation is primarily attributable to coarsening and reduction of intragranular precipitates and is also slightly related to the formation of precipitate-free zone (PFZ). Three main factors cause the unfavorable microstructure in NA-free alloy at high temperatures AA: (1) Insufficient nucleation of intragranular precipitates induced by weakened nucleation driving force, larger critical nucleation radius, and rapid vacancy annihilation; (2) The nucleated precipitates are prone to coarsening; (3) The precipitation near grain boundary is obstructed due to the depletion of vacancies and solutes. Clusters formed during NA can inhibit the unfavorable microstructure by delaying the annealing out of excess vacancies, promoting the nucleation of precipitates, and elevating the activation energy for precipitation coarsening, thereby enhancing the hardening potential. This work is instructive for the formulation of heat treatment strategies for Al–Mg–Zn–Cu alloys with high Mg/Zn ratios.

1. Introduction

Low-density aluminum alloys are usually considered to be the preferred candidates for lightweight components in engineering sectors such as transportation and aerospace, etc.; nevertheless, mainstream commercial aluminum alloys gradually cannot meet the increasingly rigorous performance requirements [1]. Hence, it is highly urgent to develop aluminum alloys with better performance. Recently, Al–Mg–Zn–Cu alloys with high Mg/Zn ratios (>1) have gained significant attention for their desirable synergy of adequate corrosion resistance, excellent formability, low quench sensitivity, and superior

* Corresponding author.
E-mail address: wangqudong@sjtu.edu.cn (Q. Wang).
https://doi.org/10.1016/j.jmrt.2023.07.111

mechanical properties [2–4]. These alloys have exhibited substantial application potential in automotive industries.

The dominant strengthening contributor of high-Mg/Zn-ratio Al–Mg–Zn–Cu alloys is precipitation strengthening induced by T-$Mg_{32}(Al, Zn)_{49}$ type dispersoids, and the precipitation sequence is expressed as supersaturated solid solution → GP(Guinier-Preston)I → T″ (GPII) → T′ → T [5]. Accordingly, much work has been carried out to enhance precipitation-strengthening, mainly embodied in composition regulation and heat treatment regime optimization [4,6–11]. The increase of Zn and Mg in these alloys increases the content of T phase, thus enhancing the hardening potential [7,11]. The addition of Cu can increase the growth rate and quantity of GP zones and reduce the critical nucleation radius of the strengthening phase, thus accelerating the age-hardening kinetics [8,9]. The addition of trace elements like Ag and Si exhibits similar efficacy [10,11]. On the other hand, a series of multi-stage aging strategies have been developed to considerably decrement of the time for peak aging since the required a long time for successful single-stage artificial aging (AA) is not acceptable for the industry [3,4,6,12]. A large number of pre-precipitated stable GP zones serve as the potential nucleation sites for the subsequent strengthening phases according to the kinetics for accelerated aging [1,4,9]. Moreover, the AA time can be further reduced by applying pre-strain [6,13]. However, the existing studies usually tacitly exclude the interference of natural aging (NA), which often occurs inevitably and may last minutes to months. As is well known, solute clusters that form during NA may inhibit subsequent AA responses [13–16]. Generally, such negative NA effect is attributed to two aspects: (1) NA clusters cannot promote the precipitation of the strengthening phase, but reduce solute supersaturation [14,17]; (2) the vacancy trapping associated with the formation of NA clusters reduces the effective diffusivity of solutes [18,19]. Accordingly, various strategies are implemented to alleviate the adverse effects of NA on subsequent AA. It is found that increasing AA temperature can reverse the negative NA effect of Al–Mg–Si alloys, which is attributed to the reduction of the nucleation barrier of the strengthening phase [15,16]. The addition of high solute-vacancy binding energy elements (for instance, Sn, In) significantly delayed the formation of NA clusters, thus retaining the AA hardening ability [20,21]. Pre-aging can promote the formation of stable clusters that serve as templates for the strengthening phase, thus improving the baking response of the alloy [20].

Nevertheless, these studies cannot be rigidly linked to the Al–Zn–Mg–Cu system due to the distinct precipitation behavior. The relevant knowledge regarding the influence of NA on AA in the high-Mg/Zn-ratio Al–Mg–Zn–Cu system remains limited. Cao et al. proposed that unstable clusters formed during NA dissolve at 180 °C, thereby delaying the aging kinetics and weakening the hardening response [5,12], while Lukas et al. reported an acceleration effect of NA on subsequent AA kinetics [4]. These divergent results are closely related to NA duration and AA temperatures, and necessitate further investigation to establish fundamental principles for regulating heat treatment regimes. For this purpose, this work is dedicated to scrutinizing the effects of NA on AA of Al–5Mg–3Zn–1Cu alloy.

2. Materials and methods

Pure Al, pure Mg, pure Zn, and Al–50Cu master alloys were melted in a resistance furnace, and 0.3 wt% Al–5Ti–1B master alloy was introduced for grain refinement. The melt was refined and cast in a steel mold. Subsequently, the casting was directly forged at 400 °C with a deformation degree of 50%. The samples with the size of 10 × 10 × 1 mm^3 cut from the center of the forging were solution heat-treated at 470 °C for 24 h, followed by quenching in water at 20 °C. The as-quenched samples were naturally aged for 0 h, 24 h, 240 h, and 2400 h (labeled successively by NA-free, NA-24 h, NA-240 h, and NA-2400 h). Subsequently, these samples were artificially aged at 120, 150, and 175 °C, respectively. For AA over 360 s, the samples were soaked in an oil bath for insulation, while in the case of the first 360 s of AA, the samples were immersed in a low-melting alloy melt (melting point 92 °C) preheated by the same oil bath to ensure good heat transfer efficiency. The oil bath maintained a temperature fluctuation of less than 3 °C and enabled the samples to reach the target temperatures in approximately 10 s. While for samples submerged in the low-melting alloy, they were heated to more than 95% of the target temperature within 1.5 s, and were heated to the target temperature in about 2.5 s. When conducting short-term AA experiments, add 1 s to the set time to minimize interference from the heating stage.

The alloy's compositions were measured using an inductively coupled plasma optical emission spectrometer, and the results are shown in Table 1. The as-quenched samples were mechanically ground, polished, and then etched with Keller's reagent for metallographic analysis. Additionally, the unetched sections were polished with argon ion beams for electron backscattering diffraction (EBSD) analysis. Differential scanning calorimetry (DSC) analyses were performed between 25 and 275 °C with a heating rate of 5 °C/min. Vickers hardness of the alloy was measured with a load of 2 kg and a dwell time of 15 s, the average of 5 independent measurements is reported to ensure repeatability. Uniaxial tension tests were conducted on the peak-aged alloys at a rate of 1 mm/min, and the reported results are the averages of 3 parallel tests. Transmission electron microscopy analysis (TEM) was performed on a TALOS F200X microscope, operating at 200 kV. The TEM samples were mechanically ground to about 80 μm thick and then double-jet electro-polished in a 30 vol% nitric acid methanol solution at −25 °C.

3. Results

3.1. Microstructures before AA

Fig. 1(a–c) shows the microstructure of the alloy prior to AA. The metallograph (Fig. 1(a)) displays complete dissolution of

Table 1 – Chemical compositions of the alloy (wt.%).

Element	Mg	Zn	Cu	Ti	Al
Concentration (wt.%)	5.07	3.01	1.11	0.01	Bal.

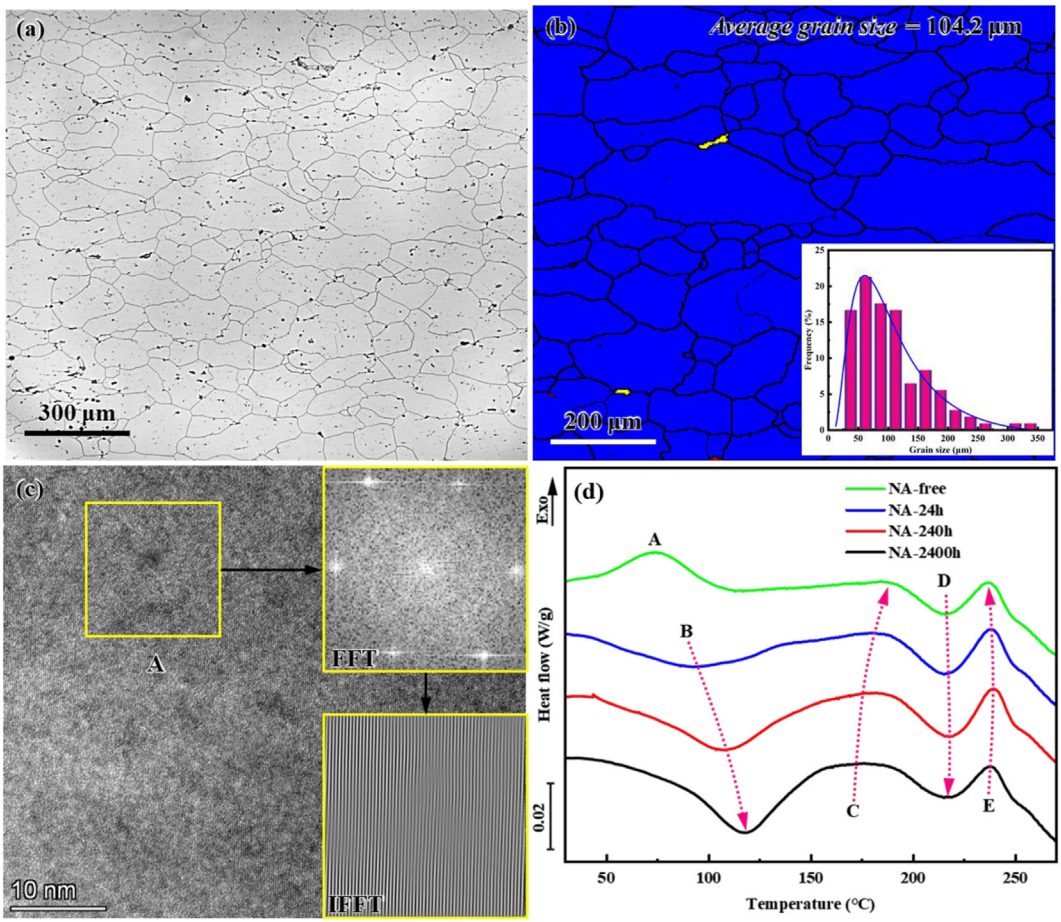

Fig. 1 – Microstructure of the alloy before AA: (a) metallograph and (b) recrystallization map of the NA-free alloy, (c) HRTEM image of the NA-2400 h alloy, and (d) DSC curves of the alloys before AA.

the second phase into the matrix. In this study, to avoid the interference of pre-existing dispersoids on aging, no recrystallization inhibitor was introduced, resulting in a fully recrystallized grain structure with an average size of 104.2 μm, which is visible in the recrystallization map and corresponding grain size distribution (Fig. 1(b)). Fig. 1(c) highlights the formation of clusters during NA, with the fast Fourier transform (FFT) and inverse FFT (IFFT) images indicating that the clusters in the NA-2400 h alloy are fully coherent with the matrix.

Fig. 1(d) illustrates the DSC thermograms of the alloys before AA. The exothermic peak A at 75 °C corresponds to GP zone formation [5,22], and the endothermic peak B located near 100 °C is attributed to the dissolution of NA clusters [22,23]. The peak C between 150 and 185 °C corresponds to the formation of T′ precipitates. Peak D near 220 °C and peak E near 240 °C correspond to the dissolution of T′ precipitates and the formation of T precipitates, respectively [7]. Peak A only exists on the DSC curve of the NA-free alloy. With NA proceeding, peak B shifts to higher temperatures (from 92.5 to 118.7 °C), and the relevant enthalpy also increases (from 5.75 to 12.6 J/g), implying increased cluster stability and fraction [23,24]. On the other hand, the wide temperature range corresponding to peak C indicates that the precipitation of the T′ phase covers a wide temperature range. NA has marginal effects on peaks D and E.

3.2. *Age-hardening behavior*

Fig. 2 depicts the hardness evolution of the alloy during room-temperature storage. Following a brief incubation period (~0.5 h), the hardness rose swiftly from 77.7 HV to 111.2 HV within the first 24 h of NA. Subsequently, the NA hardening decelerated and the hardness reached 124.8 HV after 240 h of NA. Eventually, the hardness of the alloy tends to stabilize at 135.5 HV after 2400 h of NA. Such hardness evolution has been generally observed in Al–Mg–Zn–Cu alloys [25,26].

Fig. 3(a–c) illustrates the age-hardening behavior of the alloys at 120, 150, and 175 °C, respectively. The NA-free alloy hardened constantly, while the naturally-aged alloys experienced a short softening stage before hardening. Interestingly, the NA-free alloy hardens more slowly at high temperatures, consistent with previous observations in Al–Mg–Si alloys [27,28]. In the case of peak-aging, the corresponding time to peak hardness and peak hardness was illustrated in Fig. 3(d & e), the alloys were hardened to comparable peak hardness (~177 HV) at 120 °C with the same aging time (160 h). However, at 150 °C, the NA-240 h and NA-2400 h alloys achieved higher

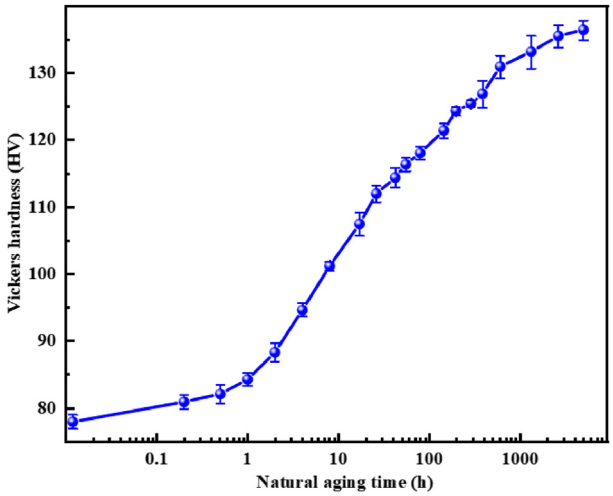

Fig. 2 – Hardening curve of the alloy during NA.

peak hardness in a shorter aging time than NA-free and NA-24 h alloys. Raising AA temperature to 175 °C further exacerbated such disparity. Similar differences in hardening response were also observed in AA7075 alloy with unconventionally small grains [29]. Note that reversion of NA occurred in the initial stages of AA, as is universally observed in heat-treatable alloys [23,30]. As shown in Fig. 3(f & g), the most-reverted hardness increases with the extension of NA time and the decreasing of AA temperature, and the time to reach the most-reverted hardness is following the same trend.

3.3. *Mechanical properties*

Fig. 4(a–c) shows the tensile curves of the peak-aged alloys, and the corresponding yield strength (YS) is illustrated in Fig. 4(d). YS strongly depends on NA time and AA temperature. During 120 °C aging, all alloys attained comparable YS; however, as AA temperature shifts to 150 °C, the YS of NA-free and NA-24 h alloys decreased significantly compared with that of NA-240 h and NA-2400 h alloys, with a differential of about 58.1 MPa. Elevating the AA temperature to 175 °C further aggravates the YS loss to approximately 120.8 MPa. The YS results echo the peak hardness finding in section 3.2.

3.4. *Microstructure*

3.4.1. *Microstructure of the alloy peak-aged at low temperature*

The microstructure of the alloy during AA was characterized to elucidate the otherness in hardening behavior. Fig. 5 depicts the microstructure of the alloy peak-aged at 120 °C, and the size distribution of the intragranular precipitates is summarized in Fig. 6. Substantially, there is no distinct difference in intragranular morphologies. The selected area diffraction patterns (SADPs, insets in Fig. 5(a & b)) demonstrate that the types of precipitates are consistent, and their size and quantity density are also equivalent (Fig. 6). There is a slight difference in grain boundary morphology between NA-free and NA-2400 h alloys. A narrow precipitate-free zone (PFZ) with a width of 24 nm in the NA-free alloy and a narrow precipitate-sparse zone (PSZ) with a width of 31 nm in the NA-2400 h alloy were observed, respectively. There are fine precipitates in PSZ, which have an equivalent size to those within the matrix away from the grain boundary but with a much lower density. The grain boundaries of both alloys were decorated with sporadic fusiform precipitates (GBPs). Compared with NA-2400 h alloy, the GBPs in NA-free alloy are coarser, but relatively less, as shown in the insets in Fig. 5(c & d). Substantially, the difference in microstructure between NA-free and NA-2400 h alloy after peak-aging at 120 °C is not significant, indicating that NA has a marginal effect on the microstructure evolution at low AA temperatures, which is consistent with the corresponding hardening responses.

3.4.2. *Microstructure evolution of the alloy at high AA temperature*

In contrast, NA has a significant effect on the microstructure evolution at high AA temperatures. Fig. 7 shows the evolution of intragranular precipitates of the NA-free and NA-2400 h alloys during aging at 175 °C. In both alloys, precipitates were observed at the germination stage (30 s) of AA and grow continuously with the aging proceeding. It is found that the precipitates in NA-free alloy are much coarser and sparser at any stage, and this difference is very striking even in the germination stage of AA. Concretely in Fig. 6, the size of precipitates at the germination stage, early stage (0.5 h), and peak-aging state for NA-free alloy are 11.4 nm 14.1 nm and 20.1 nm, respectively, such precipitate sizes were sequentially reduced to 3.1 nm, 5.4 nm and 8.4 nm for NA-2400 h alloy. Moreover, the species of the precipitates at the early stage of aging were also different, although the precipitates in both alloys under peak-aging state are identified as T′ phase. The diffraction spots of T′ precipitates can be observed at the germination stage of AA for NA-free alloy, but they cannot be identified for NA-2400 h alloy even after aging for 0.5 h.

Furthermore, HRTEM analysis was conducted to distinguish the specific precipitates at the early stage of AA, the results are illustrated in Fig. 8. For NA-free alloy, spherical and faceted precipitates were observed (Fig. 8 (a)) in the germination stage of aging (marked as A and B), respectively, and two sets of diffraction spots were observed near $<\bar{1}1\bar{1}>_{Al}$ direction on the SADP. The FFT images demonstrate that the diffraction spots of spherical precipitate A are aligned straightly along the $<\bar{1}1\bar{1}>_{Al}$ direction (Fig. 8 (a1)), which corresponds to the T″ phase based on our previous work [2]. Conversely, the diffraction spots of faceted precipitate B slightly deviated from $<\bar{1}1\bar{1}>_{Al}$ direction (Fig. 8 (a2)), which belongs to T′ phase [2]. The precipitate specie does not change after slightly extending the AA time, as depicted in Fig. 8 (b). While for NA-2400 h alloy (Fig. 8(c)), irregular-shaped precipitates (designated as E) in addition to spherical T″ precipitates (F) were observed. No extra diffraction spots were found on the corresponding FFT pattern (Fig. 8(c1)), so these precipitates were designated as GP zones. Note that only diffraction spots of T″ precipitates were found after 0.5 h of AA (Fig. 9(d)), implying that the GP zones transformed into T″ phase completely.

Apart from intragranular precipitates, NA also significantly impacted the grain boundary morphology. Fig. 9 exhibits the

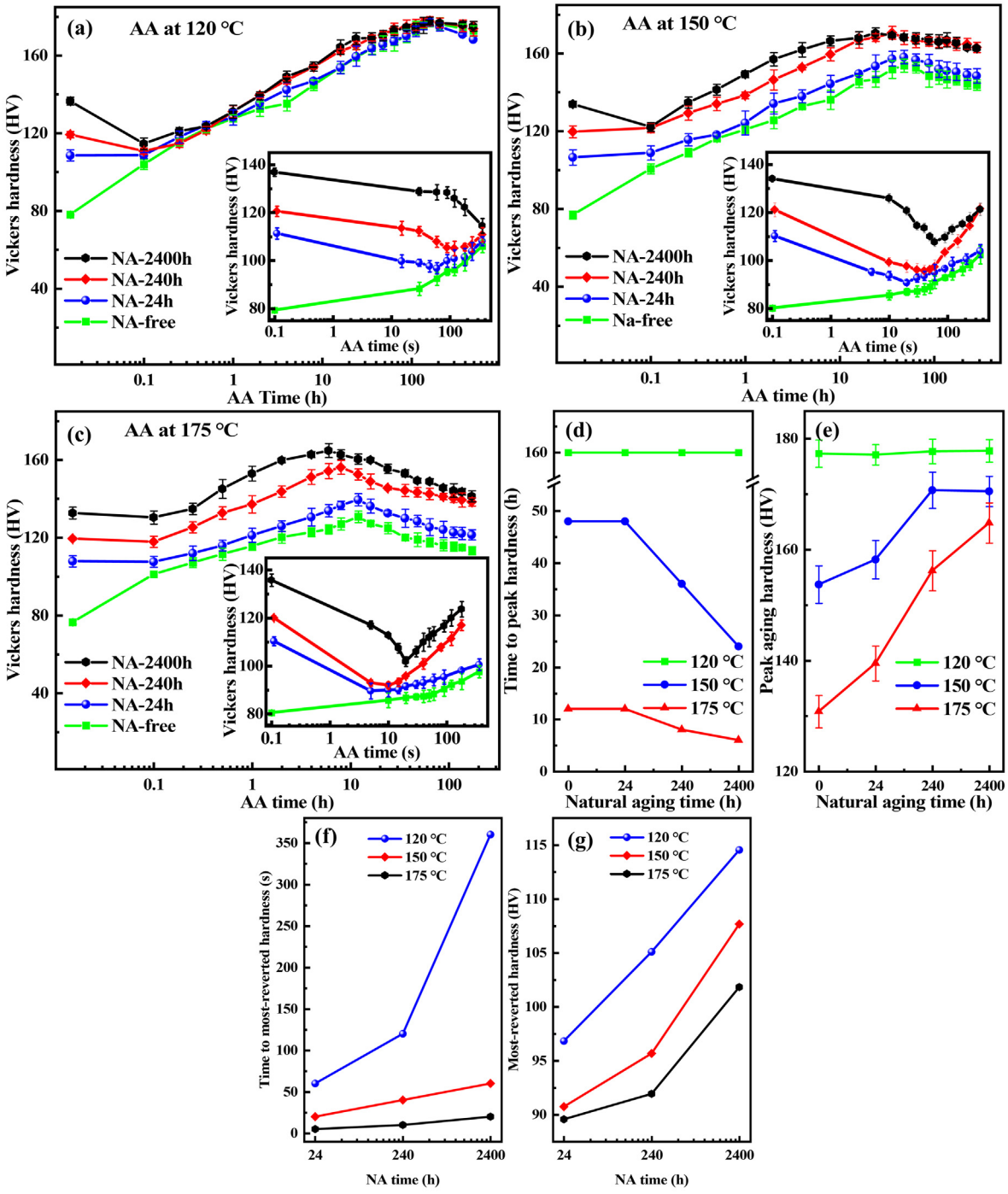

Fig. 3 – Hardening curves of the alloys at (a) 120 °C, (b) 150 °C, (c) 175 °C, (d) time to peak hardness, (e) peak aging hardness, (f) time to reach most-reverted hardness, and (g) most-reverted hardness during the reversion stage.

intergranular morphology of the alloys at various AA stages. The observed regions were selected at random, therefore, the obtained morphology represents the general situation inside the samples. For the same AA conditions, the selected zone axis for grain boundary morphology observation is consistent. The difference in grain boundary morphology has already been manifested even in the germination stage of aging. For NA-free alloy, continuous grain boundary precipitates begin to form and a precipitate-free zone as wide as 116 nm emerged after 30 s of short aging (Fig. 9(a)). With the aging proceeding, a large number of precipitates formed at grain boundaries, which slightly widened the PFZ to 133 nm (Fig. 9(b)). The PFZ in the alloy after 175 °C AA is much wider than that after 120 °C AA. Finally, after peak aging, the grain boundaries were filled with coarse precipitates, and the PFZ is further widened to 165 nm (Fig. 9(c)). In contrast, in NA-2400 h alloy, no trace of

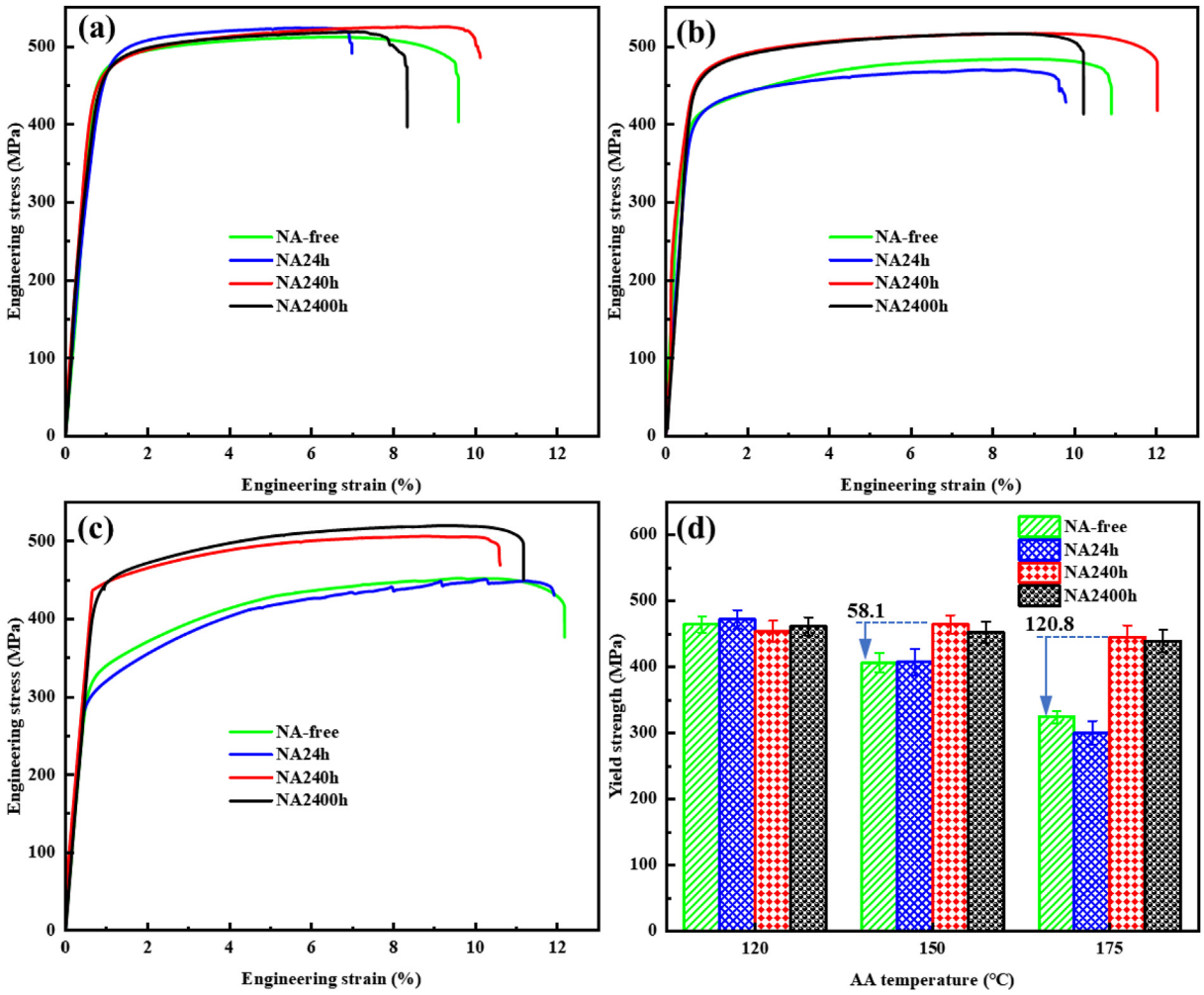

Fig. 4 – (a) Tensile curves of the alloys peak-aged at (a) 120 °C, (b) 150 °C, (c) 175 °C, and (d) the corresponding yield strength.

PFZ was found at the early stage of aging, and only a small amount of precipitates were discreetly distributed at grain boundaries (Fig. 9(d and e)). Therefore, in the peak-aged alloy, only a PSZ with a width of 132.5 nm was observed, in which hybrid sporadic coarse precipitates and dispersed fine precipitates were distributed (Fig. 9(f)).

4. Discussion

The above microstructure observation echoes well with the age-hardening responses. At low AA temperature (120 °C), NA has a marginal influence on the peak-aged microstructure and thus hardly changes the hardening response. Conversely, at high AA temperatures (above 150 °C), short-term NA (24 h) hardly affects AA behavior, but NA over 240 h has an accelerating and consolidating effect on the follow-up AA, because NA inhibits the coarsening and reduction of intragranular precipitates and prevents the formation of PFZs. The dependence of such NA effect on NA time and AA temperature is analyzed emphatically in the following sections.

4.1. *Effect of NA on precipitation in grains interior*

Microstructure characterization of the alloy in the early aging period emphasized that the intrinsic influence of NA persists in incipient AA, implying that NA affects the nucleation of precipitates during AA [14]. Essentially, precipitation during aging involves diffusion-type phase transformation process assisted by vacancy-solute exchange [31]. Both vacancy and solute are supersaturated after quenching, which is theoretically conducive to the nucleation of precipitates based on classical nucleation theory [32]. However, excess vacancies are prone to annihilation, thus the actual nucleation degree is a compromise between excess vacancy annihilation and stimulated solute diffusion [27]. For direct AA, precipitation is not affected at low temperatures, but limited nucleation of precipitates is observed at high temperatures (Fig. 7 (a)). Dual-sided factors lead to inhibited nucleation in the generation stage of aging at high temperatures. On the one hand, according to classical nucleation theory [33,34], as AA temperature rises, the solutes supersaturation decreases drastically, while the critical nucleation radius increases, resulting in the difficulty of nucleation. On the other hand, the temperature-

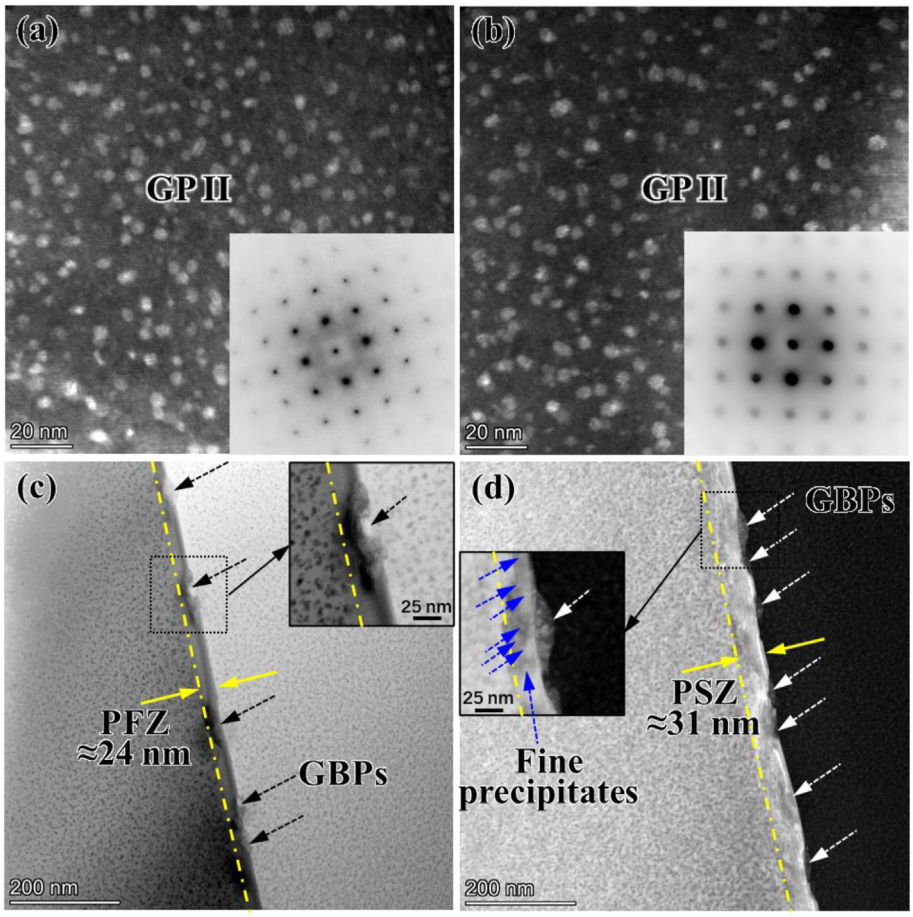

Fig. 5 – Intragranular (a, b) and intergranular (c, d) morphology of the NA-free (a, c) and NA-2400 h (b, d) alloys after peak-aging at 120 °C.

dependent annihilation of vacancies has to be considered [27,35]. At low temperatures, the relatively slow annihilation speed ensures that sufficient nuclei have been formed before the vacancy concentration falls to the equilibrium value. Cao et al. attributed the coarsening of precipitates during direct AA to the faster attachment of solute to the existing precursor driven by a large number of excess vacancies [3]; however, the effect of vacancy annihilation has been overlooked. In this study, as analogously mentioned in Ref. [27], the vacancy concentration in the bulk matrix decays rapidly to the equilibrium level at high temperatures, resulting in a low nucleation rate and marginal hardening [27,36]. Evidence supporting this perspective includes the fact that at the beginning of AA, the hardness increases faster at low temperatures for NA-free alloy (inserts in Fig. 3(a–c)). Yang et al. attributed this abnormal phenomenon to the reduced efficiency of assisting solute jump caused by rapid annealing out of excess vacancies [27].

During NA, the excess vacancies and solutes undergo a distinctly different evolution from that during AA: solute-vacancy complexes form, and further grow or coalesce into clusters during NA [37,38], which are driven primarily by excess vacancies [27]. According to Zurob, the growth of clusters is accompanied by the capture of excess vacancies [19]. Since the rate of excess vacancy escaping from the clusters is the rate-limiting step of cluster growth, it can be deduced that most of the excess vacancies are entrapped in the clusters after long-term NA. These solute clusters formed during NA hardened the alloy, as shown in Figs. 1 (c) and Fig. 2. Esmaeili pointed out that the square of the hardening degree (ΔH) is proportional to the relative volume fraction (f) of the clusters [39]:

$$\Delta H^2 \propto f \tag{1}$$

ΔH is defined by linear normalizing the actual hardness (H) between the as-quenched hardness (H_{AQ}) and the saturated hardness (H_{NA}) after long-term NA:

$$\Delta H = \frac{H - H_{AQ}}{H_{NA} - H_{AQ}} \tag{2}$$

In the early stage of AA, the reversion of NA occurs and the cluster dissolves, the corresponding kinetics can be expressed as:

$$f = \left(1 - Bt^{1/2}\right)^3 \tag{3}$$

where t is AA time, B is a thermal activation parameter and can be expressed as:

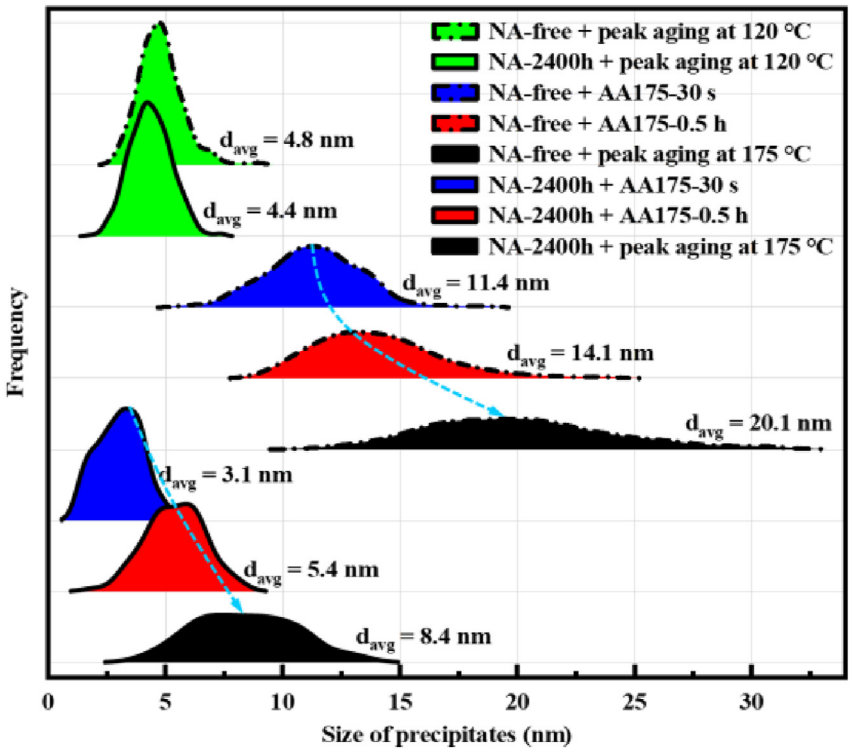

Fig. 6 – The size distribution of the intragranular precipitates in the alloys.

$$B = B_0 \exp(-Q_{diss}/RT) \quad (4)$$

where B_0 is the pre-exponential factor, Q_{diss} is the apparent activation energy of dissolution of NA clusters, R is the universal gas constant, and T is AA temperature. The hardness during the reversion of NA is fitted using the least-square algorithm. Fig. 10 shows the relationship between B and NA time and AA temperature, and Q_{diss} is derived from the fitting lines. Q_{diss} increases with the prolongation of NA and is stable around 54 kJ/mol after long-term NA, demonstrating that the clusters in the alloys after long-term NA are more difficult to dissolve.

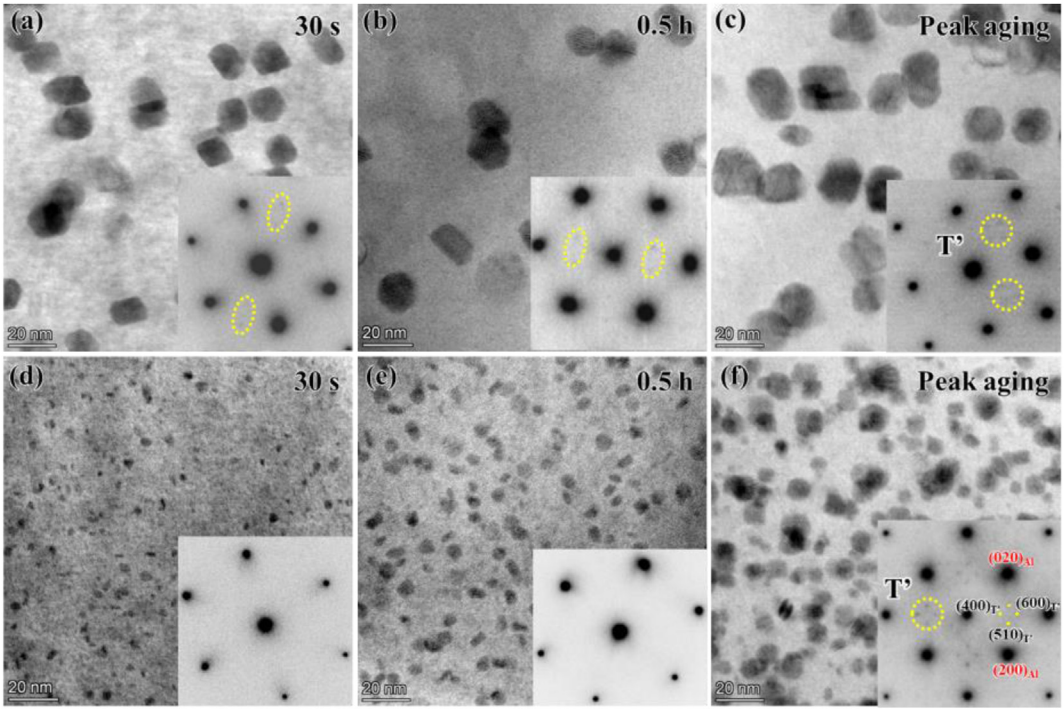

Fig. 7 – Evolution of intragranular precipitates of the NA-free (a–c) and NA-2400 h (d–f) alloys during AA at 175 °C.

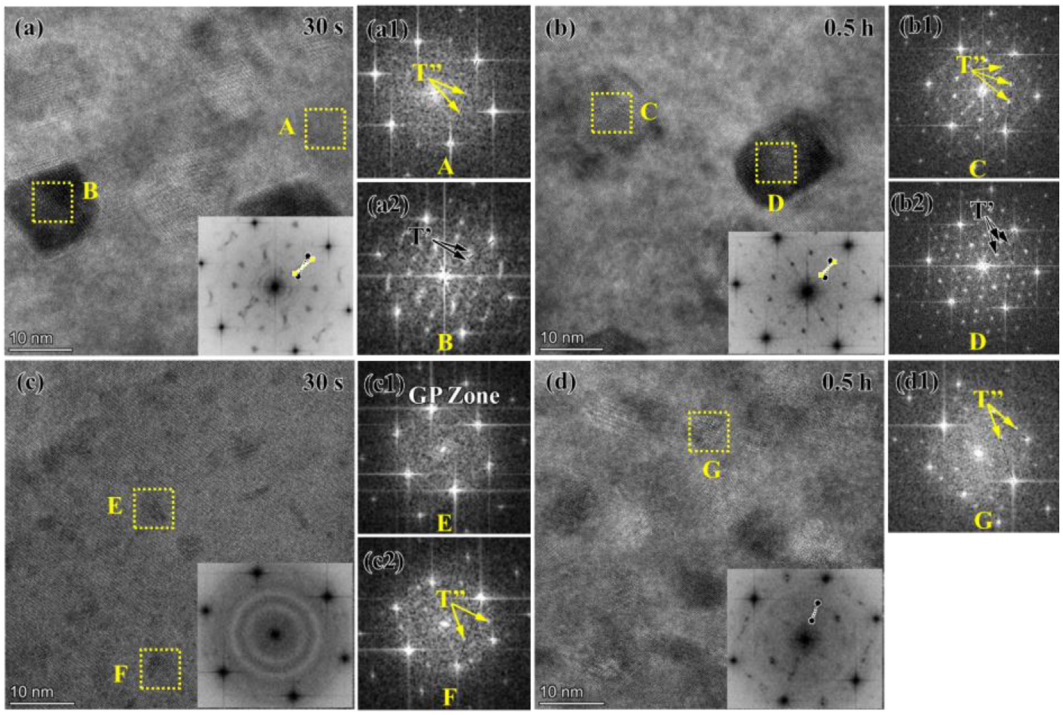

Fig. 8 – HRTEM images of the NA-free (a, b) and NA-2400 h alloy (c, d) after aging at 175 °C for 30 s (a, c) and 0.5 h (b, d), the attached figures are FFT images of typical precipitates, the viewing direction is < 011>$_{Al}$.

When the alloys are subjected to AA after NA, the stability of clusters is particularly important. On the one hand, stable clusters may serve as nuclei to facilitate the heterogeneous nucleation of precipitates [40]. On the other hand, the unstable clusters dissolve, releasing solutes and trapped vacancies [41]. According to the vacancy-prison mechanism [42], compensation of solutes and vacancies can also stimulate precipitation [3,27]. However, short-term NA did not promote subsequent AA response at either low or high temperatures, which may be closely related to the dissolution of unstable

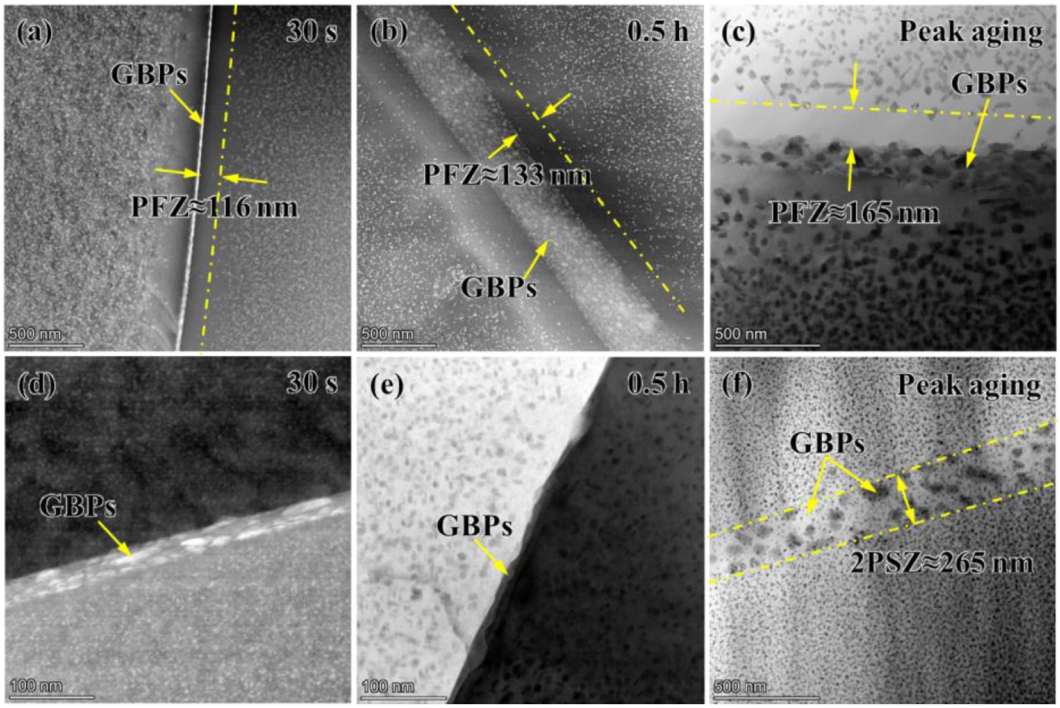

Fig. 9 – Evolution of grain boundary morphology in the NA-free (a–c) and NA-2400 h (d–f) alloys during aging at 175 °C.

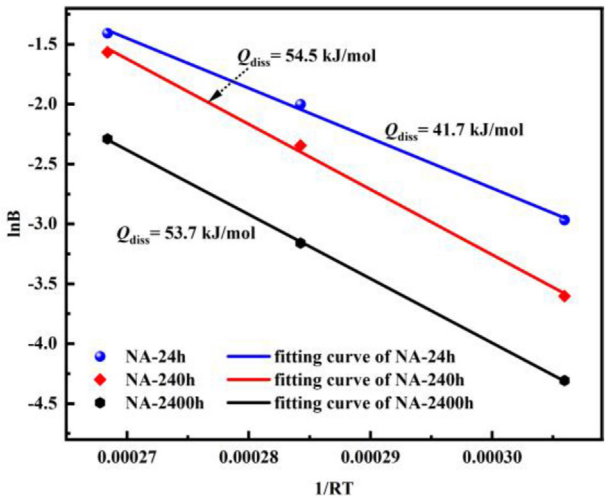

Fig. 10 – Plot of lnB-1/RT.

clusters in the alloy. According to Lee et al.'s measurements and calculations [43], even after long-term NA, the difference in solute content in the matrix between the natural-aged and the as-quenched states in Al–Mg–Zn–Cu alloy is not significant. Therefore, for the insufficiently decomposed NA-1h alloy, the matrix is still highly supersaturated before AA, which means that the strengthening phase will precipitate from the matrix at the same time as the reversion of NA [44]. Therefore, the hardness evolution in the early stage of AA is an apparent result of competition between precipitation-induced strengthening and reversion-induced weakening [45]. Assuming that the matrix precipitation behavior of NA-24 h alloy during the reversion stage is similar to that of as-quenched alloy, after deducting the hardening increment induced by matrix precipitation based on Fig. 3, the difference in hardness between most-reverted NA-24 h alloy and the as-quenched alloy is very small. I. KOVÁCS et al. [46,47] indicated that for completely reversed alloys, although their microstructure characteristics are already very similar to the solid solution state, the mechanical properties will still be slightly higher than the as-quenched state. Therefore, the reversion of NA clusters of NA-24 h alloy is very thorough in this study. Therefore, the most-reverted NA-24 h alloy can be considered in a quasi-solid solution state with concentration fluctuations, where cluster dissolution leads to local solute enrichment [44]. The higher the AA temperature, the more complete the dissolution of clusters, and the microstructure in the most-reverted alloy is more similar to that of the solid solution state. Hence, the local solute enrichment induced by the dissolution of NA clusters is mainly responsible for the precipitation of the strengthening phase in the early stage of AA. Therefore, the precipitation behavior of NA-free alloy and NA-24 h alloy during AA is similar from the perspective of microstructure evolution, as precipitates are essentially formed from the supersaturated matrix. Moreover, even if a small number of NA clusters survive at low temperatures, the sluggish diffusion of solute and vacancy delays the growth of precipitates.

Conversely, for long-term NA, most of the clusters are preserved at low AA temperatures, which is conducive to the precipitation nucleation but decreases the solute supersaturation that directly determines the critical driving force [48]. These two contradictory aspects eventually lead to a small influence of long-term NA on the following AA kinetics at low temperatures. While at high AA temperatures, although most of the NA clusters tend to be dissolved, this process compensates for the solute and vacancy concentration in the matrix. More importantly, this process also delays the annealing out of excess vacancies, thereby stimulating solute jump. Therefore, a pronounced nucleation behavior was observed, as elucidated by the vacancy prison mechanism [42].

This vacancy/cluster-related NA effect can also well explain the difference between the results of this study and similar work. In Ref. [29], no NA-induced refinement and densification of the precipitates after AA was observed in ultrafine-grained AA7075 alloy, which is attributed to the more prompt annihilation of released vacancies induced by higher grain boundary density [35]. In contrast, the lower Cu content in Al-5.1Mg-3.0Zn-0.8Mn-0.15Cu alloy lead to insufficient stability of the clusters and thus failed to facilitate AA response at 180 °C [5,9].

Interestingly, NA seems to alter the precipitation sequence at high temperatures (Fig. 8). T′ precipitates were found in NA-free alloy at the budding stage of 175 °C AA, these precipitates are likely to be formed directly from the matrix. Similar results have also been reported in Al–Mg–Si alloys [48], and its internal mechanism is also related to vacancy partitioning [49]. It has proved that the strengthening ability of the T′ phase is weaker than the T″ phase [40], therefore, the easier formation of T′ phase may also be an important reason for the lower hardening kinetics of NA-free alloys during high-temperature AA.

The positive impact of NA on AA is also reflected in the hardening stage, which mainly involves the growth of precipitates. A quantitative analysis of the hardening kinetics of the alloy was conducted based on the JMAK model [28]:

$$\left(\frac{H - H_{AQ}}{H_{peak} - H_{AQ}}\right)^2 = 1 - \exp(-kt^n) \tag{5}$$

where H_{peak} represents the hardness at the peak-aging state, and n is the Avrami exponent. k is the rate constant and is expressed in the form of the Arrhenius equation:

$$k = k_0 \exp(-Q_{AA} / RT) \tag{6}$$

where k_0 and Q_{AA} are the pre-exponential factor and the AA activation energy, respectively. Based on Eq. (5), normalization and least squares fitting are performed on the hardness values before peak-aging (Fig. 3(a–c)). The correlation between each fitting curve and corresponding experimental values was more than 0.95. The calculated n is around 0.5. Fig. 11 shows the relationship between k and NA time and AA temperature, when AA at low temperature (120 °C), k increased slightly with the extension of NA. However, when the aging temperature rose to above 150 °C, the temporary NA (24 h) caused a slight increase in k value, but when the alloy was naturally aged beyond 240 h, k increased sharply. Such results indicate that the precipitation kinetics can be enhanced only when the alloy has been naturally aged for a long time and artificially aged at high temperatures, implying that the growth behavior of precipitates is also unique under

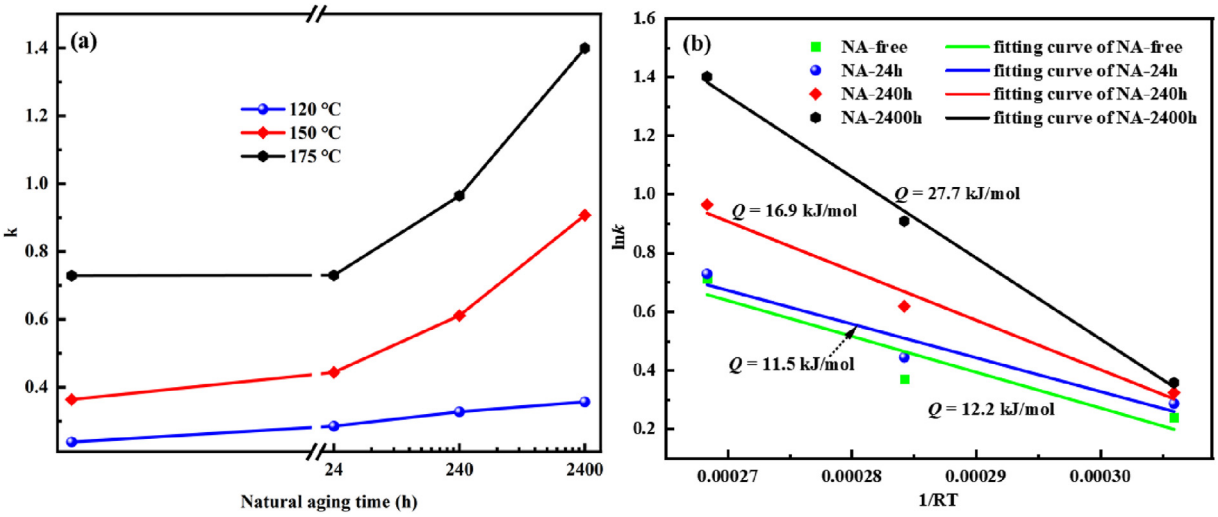

Fig. 11 – The relationship between *k* and NA time (a) and AA temperature (b).

such circumstances. As shown in Fig. 11(b), the Q_{AA} was derived from the ln*k*-1/RT plot. Since the calculated interval mainly involves the growth of precipitates, Q_{AA} quantified the resistance of precipitate growth. Q_{AA} of NA-free and NA-24 h alloys are equivalent, about 12 kJ/mol. With the extension of NA, Q_{AA} rises steadily to 16.9 and 27.7 kJ/mol for NA-240 h alloy and NA-2400 h alloy, indicating that NA inhibits the coarsening of precipitates by elevating the activation energy of precipitate growth. This is consistent with Cao et al. that the T′ phase precipitated directly from the matrix at high temperatures is easier to be coarsened [3].

4.2. *Effect of NA on PFZ formation*

The PFZ with poor deformation resistance is detrimental to the mechanical properties of alloys [50] and is demonstrated to be the culprit of the strength loss of ultrafine-grained AA7075 alloy, in which PFZ occupies a high proportion of whole grain (~19–27%) [29]. The coarse grains observed in this study have a low (less than 0.5%) PFZ proportion, so PFZ is not recognized as the decisive factor for strength reduction. However, it is still worth analyzing the influence of NA on PFZ formation because it can prove the strong vacancy behavior dependence of microstructure characteristics. Presently, there are two mainstream explanations for the formation of PFZ, namely vacancy depletion and solute depletion mechanisms [51]. The vacancy depletion theory suggests that even if the solute is supersaturated, precipitation in the vicinity of grain boundary is inhibited because the vacancy concentration in these regions is lower than the critical value for precipitation nucleation due to the preferential migration of vacancies towards the grain boundary [52]. On the other hand, the solute depletion theory suggested that the PFZ generation is dominated by the reduced solute supersaturation near the grain boundary due to the enrichment of solute towards the grain boundary [53]. In this study, grain boundary is regarded as the most efficient vacancy sink [35]. For direct AA, excess vacancies tend to migrate promptly to sinks and annihilate [27,35], thus a vacancy depletion zone (VDZ) forms near the grain boundary at the beginning of AA [29,54,55], and precipitation is suppressed in VDZ. At low AA temperatures, sporadic GBPs indicate that solute is not large-scale enriched here, which is attributed to low solute diffusion capacity. From this perspective, the PFZ at low temperatures only embodies vacancy depletion. Similarly, at high AA temperature, a wide PFZ is observed at the beginning of aging, although solute enrichment at grain boundaries was not severe (Fig. 9 (a)). This indicates that vacancy depletion is the main cause of PFZ formation at the germination stage of AA because the diffusion distance of vacancy is greater than that of solute [29]. However, as AA progresses, PFZ is only slightly broadened, but solutes accumulate in large quantities at grain boundaries, forming abundant precipitates. This phenomenon suggests that the main controlling factor of PFZ formation has shifted to solute depletion. Therefore, the PFZ at high temperatures is the result of both solute and vacancy depletion [35,56,57]. In terms of AA after NA, clusters facilitate precipitation in the vicinity of grain boundaries, as discussed in section 4.1, thus avoiding the formation of PFZ [52].

4.3. *Conceptualized microstructural evolution*

Summarily, the co-evolution of solute, vacancy, and cluster during NA and incipient AA causes the unique NA effect on Al–5Mg–3Zn–1Cu alloy [58,59], which is schematically illustrated in Fig. 12. For direct AA, the nucleation driving force and critical nucleation radius decrease and increase with increasing temperature, respectively, and the nucleation of precipitates is also influenced by the compromise between solute diffusion and annihilation rate of excess vacancies. At low AA temperatures, the excess vacancies are annealed out slowly, and they are more prone to be captured by solutes, thus ensuring a sufficient nucleation rate without considerable influence on precipitation in grain interiors. While at high AA temperatures, rapid annealing out of excess vacancies inhibited the nucleation of precipitates, and the high solute diffusivity led to the rapid coarsening of precipitates. Additionally, vacancy depletion

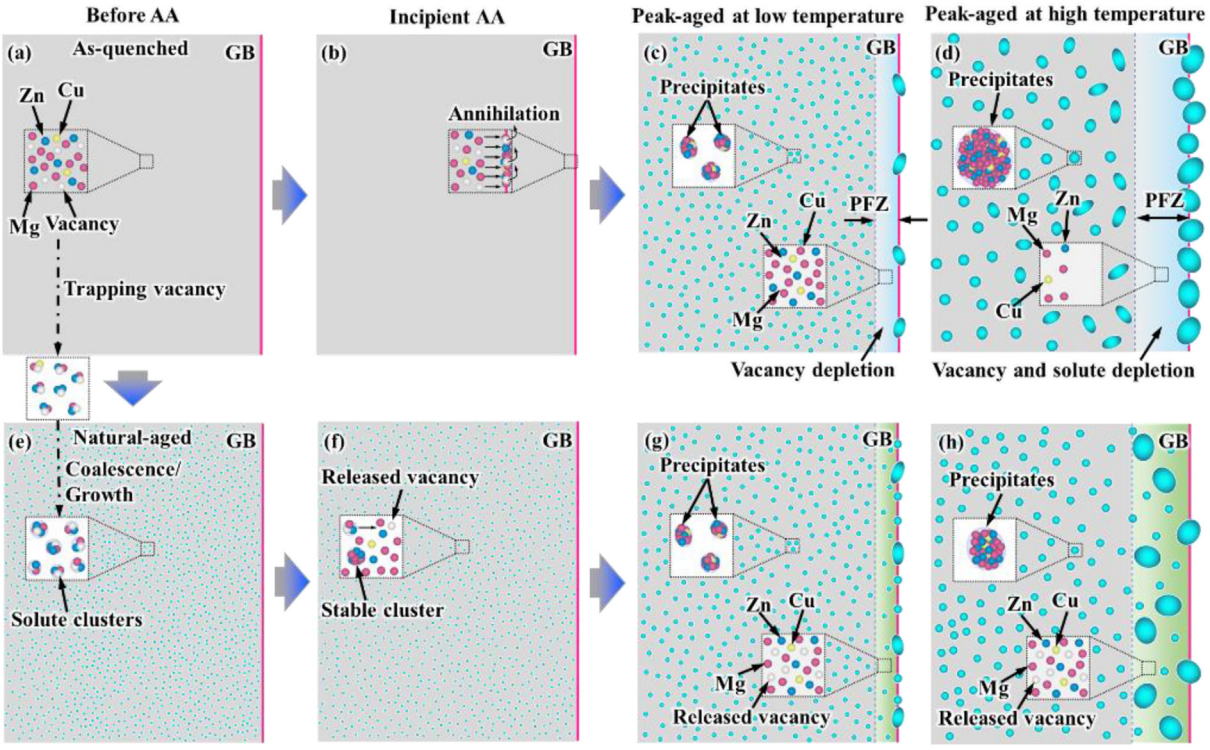

Fig. 12 – Schematic diagram illustrating the microstructure evolution of the alloy during direct AA: (a) as-quenched, (b) incipient AA, peak-aged at (c) low temperature, and (d) high temperature and AA after NA: (e) natural-aged, (f) incipient AA, peak-aged at (g) low temperature, and (h) high temperature.

results in the formation of PFZ at low AA temperature, while the formation of PFZ at high AA temperature is mainly attributed to vacancy depletion at the early stage but solute depletion at the later stage of AA. The alloy after short-term NA returns to a quasi-solid solution state at the initial stage of AA, so the final AA response differs little from that of the NA-free alloy. In the case of long-term NA, the relatively stable clusters alter the evolution pathway of excess vacancy. At low AA temperatures, although the stable NA clusters can promote the heterogeneous nucleation of precipitates, they also reduce the solute supersaturation, thus elevating the nucleation barrier of precipitates directly decomposing from the matrix. Therefore, the final microstructure and mechanical properties are close to those of the NA-free alloy. At high AA temperatures, the explosive dissolution of the clusters simultaneously supplements the solute and vacancy concentration, thus promoting the nucleation of the precipitate. At the same time, NA also elevates the activation energy for precipitate growth, thereby avoiding the precipitate coarsening.

5. Conclusions

Effects of NA on AA behavior of Al–5Mg–3Zn–1Cu alloy were studied. Short-term NA (24 h) has marginal effects on AA at any temperature, as well as long-term NA (>240 h) on low-temperature AA (120 °C). Long-term NA can accelerate AA kinetics and alleviate severe hardening capacity attenuation at high temperatures (>150 °C). Such attenuation is mainly attributed to coarsening and reduction of intragranular precipitates and is also slightly associated with the formation of wide PFZ. Three main factors cause the microstructure that is not conducive to hardening of NA-free alloy: (1) At high temperatures, the nucleation driving force of intragranular precipitates weakens, the critical nucleation radius increases, and vacancies rapidly annihilate, resulting in insufficient nucleation; (2) The precipitates are easier to coarsening; (3) The precipitation near the grain boundary is obstructed due to the depletion of vacancies and solutes. Clusters formed during NA can avoid the above-mentioned unfavorable microstructure by delaying the annealing out of excess vacancies, promoting the nucleation of precipitates, and elevating the activation energy for precipitation coarsening, thereby accelerating aging kinetics and enhancing the hardening potential.

Declaration of competing interest

The authors declare that they have no known competing financial interests or personal relationships that could have appeared to influence the work reported in this paper.

Acknowledgments

The study is supported by the National Natural Science Foundation of China (Nos. U1902220, 51674166), the National

Key Research and Development Program of China (No. 2021YFB3701303) and SJTU-Warwick Joint Seed Fund (No. SJTU2210).

REFERENCES

[1] Stemper L, Tunes MA, Tosone R, Uggowitzer PJ, Pogatscher S. On the potential of aluminum crossover alloys. Prog Mater Sci 2022;124:100873. https://doi.org/10.1016/j.pmatsci.2021.100873.

[2] Tang H-P, Wang Q-D, Luo C, Lei C, Liu T-W, Li Z-Y, et al. Effects of aging treatment on the precipitation behaviors and mechanical properties of Al-5.0Mg-3.0Zn-1.0Cu cast alloys. J Alloys Compd 2020;842:155707. https://doi.org/10.1016/j.jallcom.2020.155707.

[3] Cao C, Zhang D, Zhuang L, Zhang J. Improved age-hardening response and altered precipitation behavior of Al-5.2Mg-0.45Cu-2.0Zn (wt%) alloy with pre-aging treatment. J Alloys Compd 2017;691:40–3. https://doi.org/10.1016/j.jallcom.2016.08.206.

[4] Stemper L, Mitas B, Kremmer T, Otterbach S, Uggowitzer PJ, Pogatscher S. Age-hardening of high pressure die casting AlMg alloys with Zn and combined Zn and Cu additions. Mater Des 2019;181:107927. https://doi.org/10.1016/j.matdes.2019.107927.

[5] Hou S, Liu P, Zhang D, Zhang J, Zhuang L. Precipitation hardening behavior and microstructure evolution of Al–5.1Mg–0.15Cu alloy with 3.0Zn (wt%) addition. J Mater Sci 2018;53:3846–61. https://doi.org/10.1007/s10853-017-1811-1.

[6] Stemper L, Tunes MA, Dumitraschkewitz P, Mendez-Martin F, Tosone R, Marchand D, et al. Giant hardening response in AlMgZn(Cu) alloys. Acta Mater 2021;206:116617. https://doi.org/10.1016/j.actamat.2020.116617.

[7] Cao C, Zhang D, He Z, Zhuang L, Zhang J. Enhanced and accelerated age hardening response of Al-5.2Mg-0.45Cu (wt%) alloy with Zn addition. Mater Sci Eng, A 2016;666:34–42. https://doi.org/10.1016/j.msea.2016.04.022.

[8] Cao C, Zhang D, Wang X, Ma Q, Zhuang L, Zhang J. Effects of Cu addition on the precipitation hardening response and intergranular corrosion of Al-5.2Mg-2.0Zn (wt.%) alloy. Mater Char 2016;122:177–82. https://doi.org/10.1016/j.matchar.2016.11.004.

[9] Zhang Z, Li Y, Li H, Zhang D, Zhang J. Effect of high Cu concentration on the mechanical property and precipitation behavior of Al–Mg–Zn-(Cu) crossover alloys. J Mater Res Technol 2022;20:4585–96. https://doi.org/10.1016/j.jmrt.2022.08.171.

[10] Zhang H, Nan Y, Guo C, Cui J. Age hardening and intergranular corrosion behavior of new type Al-4.5Mg-0.6Zn-0.5Cu-XAg(wt%) alloy. J Alloys Compd 2022;910:164767. https://doi.org/10.1016/j.jallcom.2022.164767.

[11] Mao J, Wen S, Liang S, Wu X, Wei W, Huang H, et al. Precipitation behaviors and thermal stability of Al-3.5Mg-1.0Cu alloy with co-addition of Zn and Si. J Alloys Compd 2023:169401. https://doi.org/10.1016/j.jallcom.2023.169401.

[12] Cao C, Zhang D, Zhuang L, Zhang J, Liu J. Effect of pre-aging treatment on room temperature stability of Al-5.2Mg-0.45Cu-2.0Zn alloy sheet. Xiyou Jinshu Cailiao Yu Gongcheng 2020;49:1166–70.

[13] Zou Y, Cao L, Wu X, Tang S, Guo M. Synergetic effect of natural ageing and pre-stretching on the ageing behavior in T'/η' phase-strengthened Al-Zn-Mg-Cu alloys. J Mater Sci Technol 2023;146:240–51. https://doi.org/10.1016/j.jmst.2022.10.074.

[14] Pogatscher S, Antrekowitsch H, Leitner H, Sologubenko AS, Uggowitzer PJ. Influence of the thermal route on the peak-aged microstructures in an Al–Mg–Si aluminum alloy. Scripta Mater 2013;68:158–61. https://doi.org/10.1016/j.scriptamat.2012.10.006.

[15] Yu W, He H, Zhang W, Li L, Sun C. Modulation of the natural aging effect on subsequent artificial aging in Al–Mg–Si aluminum alloys with alloying content ~ 1 wt% through temperature tuning. J Alloys Compd 2020;814:152277. https://doi.org/10.1016/j.jallcom.2019.152277.

[16] Liu CH, Lai YX, Chen JH, Tao GH, Liu LM, Ma PP, et al. Natural-aging-induced reversal of the precipitation pathways in an Al–Mg–Si alloy. Scripta Mater 2016;115:150–4. https://doi.org/10.1016/j.scriptamat.2015.12.027.

[17] Tao GH, Liu CH, Chen JH, Lai YX, Ma PP, Liu LM. The influence of Mg/Si ratio on the negative natural aging effect in Al–Mg–Si–Cu alloys. Mater Sci Eng, A 2015;642:241–8. https://doi.org/10.1016/j.msea.2015.06.090.

[18] Banhart J, Lay MDH, Chang CST, Hill AJ. Kinetics of natural aging in Al-Mg-Si alloys studied by positron annihilation lifetime spectroscopy. Phys Rev B 2011;83:014101. https://doi.org/10.1103/PhysRevB.83.014101.

[19] Zurob HS, Seyedrezai H. A model for the growth of solute clusters based on vacancy trapping. Scripta Mater 2009;61:141–4. https://doi.org/10.1016/j.scriptamat.2009.03.025.

[20] Werinos M, Antrekowitsch H, Ebner T, Prillhofer R, Curtin WA, Uggowitzer PJ, et al. Design strategy for controlled natural aging in Al–Mg–Si alloys. Acta Mater 2016;118:296–305. https://doi.org/10.1016/j.actamat.2016.07.048.

[21] Pogatscher S, Antrekowitsch H, Werinos M, Moszner F, Gerstl SSA, Francis MF, et al. Diffusion on demand to control precipitation aging: application to Al-Mg-Si alloys. Phys Rev Lett 2014;112:225701. https://doi.org/10.1103/PhysRevLett.112.225701.

[22] Dupasquier A, Ferragut R, Iglesias MM, Quasso F. Vacancy-solute association in coherent nanostructures formed in a commercial Al-Zn-Mg-Cu alloy. Phys Status Solidi 2007;4:3526–9. https://doi.org/10.1002/pssc.200675772.

[23] Liu C, Feng Z, Ma P, Zhou Y, Li G, Zhan L. Reversion of natural ageing and restoration of quick bake-hardening response in Al-Zn-Mg-Cu alloy. J Mater Sci Technol 2021;95:88–94. https://doi.org/10.1016/j.jmst.2021.03.070.

[24] Dupasquier A, Ferragut R, Liddicoat P, Moia F, Ringer SP. Positron lifetime evolution during room temperature ageing in Al-Zn-Mg-(Cu). Phys Status Solidi 2009;6:2301–3. https://doi.org/10.1002/pssc.200982068.

[25] Zhang P, Shi K, Bian J, Zhang J, Peng Y, Liu G, et al. Solute cluster evolution during deformation and high strain hardening capability in naturally aged Al–Zn–Mg alloy. Acta Mater 2021;207:116682. https://doi.org/10.1016/j.actamat.2021.116682.

[26] Lee S-H, Jung J-G, Baik S-I, Seidman DN, Kim M-S, Lee Y-K, et al. Precipitation strengthening in naturally aged Al–Zn–Mg–Cu alloy. Mater Sci Eng, A 2021;803:140719. https://doi.org/10.1016/j.msea.2020.140719.

[27] Yang Z, Banhart J. Natural and artificial ageing in aluminium alloys – the role of excess vacancies. Acta Mater 2021;215:117014. https://doi.org/10.1016/j.actamat.2021.117014.

[28] Noseda Grau V, Cuniberti A, Tolley A, Castro Riglos V, Stipcich M. Solute clustering behavior between 293K and 373K in a 6082 Aluminum alloy. J Alloys Compd 2016;684:481–7. https://doi.org/10.1016/j.jallcom.2016.05.197.

[29] Ma P, Liu C, Chen Q, Wang Q, Zhan L, Li J. Natural-ageing-enhanced precipitation near grain boundaries in high-strength aluminum alloy. J Mater Sci Technol 2020;46:107–13. https://doi.org/10.1016/j.jmst.2019.11.035.

[30] Madanat M, Liu M, Banhart J. Reversion of natural ageing in Al-Mg-Si alloys. Acta Mater 2018;159:163–72. https://doi.org/10.1016/j.actamat.2018.07.066.

[31] Esmaeili S, Vaumousse D, Zandbergen MW, Poole WJ, Cerezo A, Lloyd DJ. A study on the early-stage decomposition

in the Al–Mg–Si–Cu alloy AA6111 by electrical resistivity and three-dimensional atom probe. Phil Mag 2007;87:3797–816. https://doi.org/10.1080/14786430701408312.
[32] Tang J, Liu M, Bo G, Jiang F, Luo C, Teng J, et al. Unraveling precipitation evolution and strengthening function of the Al-Zn-Mg-Cu alloys with various Zn contents: multiple experiments and integrated internal-state-variable modeling. J Mater Sci Technol 2022;116:130–50. https://doi.org/10.1016/j.jmst.2021.12.008.
[33] Liu C, Zhou Y, Ma P, He J, Chen L. Enhanced age-hardening response at elevated temperature by natural-ageing-modified precipitation in an Al-Cu-Li-Mg alloy. Mater Char 2023;199:112791. https://doi.org/10.1016/j.matchar.2023.112791.
[34] Werenskiold JC, Deschamps A, Bréchet Y. Characterization and modeling of precipitation kinetics in an Al–Zn–Mg alloy. Mater Sci Eng, A 2000;293:267–74. https://doi.org/10.1016/S0921-5093(00)01247-8.
[35] Fischer FD, Svoboda J, Appel F, Kozeschnik E. Modeling of excess vacancy annihilation at different types of sinks. Acta Mater 2011;59:3463–72. https://doi.org/10.1016/j.actamat.2011.02.020.
[36] Werinos M, Antrekowitsch H, Kozeschnik E, Ebner T, Moszner F, Löffler JF, et al. Ultrafast artificial aging of Al–Mg–Si alloys. Scripta Mater 2016;112:148–51. https://doi.org/10.1016/j.scriptamat.2015.09.037.
[37] Ferragut R, Somoza A, Tolley A. Microstructural evolution of 7012 alloy during the early stages of artificial ageing. Acta Mater 1999;47:4355–64. https://doi.org/10.1016/S1359-6454(99)00315-8.
[38] Peng J, Bahl S, Shyam A, Haynes JA, Shin D. Solute-vacancy clustering in aluminum. Acta Mater 2020;196:747–58. https://doi.org/10.1016/j.actamat.2020.06.062.
[39] Esmaeili S, Lloyd DJ, Poole WJ. Modeling of precipitation hardening for the naturally aged Al-Mg-Si-Cu alloy AA6111. Acta Mater 2003;51:3467–81. https://doi.org/10.1016/S1359-6454(03)00167-8.
[40] Hou S, Zhang D, Ding Q, Zhang J, Zhuang L. Solute clustering and precipitation of Al-5.1Mg-0.15Cu-xZn alloy. Mater Sci Eng, A 2019;759:465–78. https://doi.org/10.1016/j.msea.2019.05.066.
[41] Falahati A, Lang P, Kozeschnik E. Precipitation in Al-alloy 6016 – the role of excess vacancies. Mater Sci Forum 2012;706–709:317–22. https://doi.org/10.4028/www.scientific.net/MSF.706-709.317.
[42] Pogatscher S, Antrekowitsch H, Leitner H, Ebner T, Uggowitzer PJ. Mechanisms controlling the artificial aging of Al–Mg–Si Alloys. Acta Mater 2011;59:3352–63. https://doi.org/10.1016/j.actamat.2011.02.010.
[43] Lee S-H, Jung J-G, Baik S-I, Seidman DN, Kim M-S, Lee Y-K, et al. Precipitation strengthening in naturally aged Al–Zn–Mg–Cu alloy. Mater Sci Eng, A 2021;803:140719. https://doi.org/10.1016/j.msea.2020.140719.
[44] Löffler H, Kovács I, Lendvai J. Decomposition processes in Al-Zn-Mg alloys. J Mater Sci 1983;18:2215–40. https://doi.org/10.1007/BF00541825.
[45] Esmaeili S, Lloyd DJ, Poole WJ. Modeling of precipitation hardening for the naturally aged Al-Mg-Si-Cu alloy AA6111. Acta Mater 2003;51:3467–81. https://doi.org/10.1016/S1359-6454(03)00167-8.
[46] Kovacs I, Lendvai J, Ungar T, Banizs K, Lakner J. INVESTIGATION OF THE EFFECT OF TWO AND THREE STEP AGING ON THE eta prime PHASE FORMATION IN Al-4. 8 wt. -% Zn-1. 2 wt. -% Mg ALLOY. 1977.
[47] Ungär T, Lendvai J, Kovács I, Groma G, Kovács-Cseténvi E. Quantitative investigation of the reversion process of GP zones in an Al-Zn-Mg alloy. Int J Mater Res 1976;67:683–7. https://doi.org/10.1515/ijmr-1976-671006.
[48] Pogatscher S, Antrekowitsch H, Uggowitzer PJ. Interdependent effect of chemical composition and thermal history on artificial aging of AA6061. Acta Mater 2012;60:5545–54. https://doi.org/10.1016/j.actamat.2012.06.061.
[49] Pogatscher S, Antrekowitsch H, Leitner H, Pöschmann D, Zhang ZL, Uggowitzer PJ. Influence of interrupted quenching on artificial aging of Al–Mg–Si alloys. Acta Mater 2012;60:4496–505. https://doi.org/10.1016/j.actamat.2012.04.026.
[50] Krol T, Baither D, Nembach E. Quantification of the detrimental effects of precipitate free zones on the yield strength of a superalloy. Scripta Mater 2003;48:1189–94. https://doi.org/10.1016/S1359-6462(02)00566-3.
[51] Jiang H, Faulkner RG. Modelling of grain boundary segregation, precipitation and precipitate-free zones of high strength aluminium alloys—I. The model. Acta Mater 1996;44:1857–64. https://doi.org/10.1016/1359-6454(95)00317-7.
[52] Ogura T, Hirosawa S, Cerezo A, Sato T. Atom probe tomography of nanoscale microstructures within precipitate free zones in Al–Zn–Mg(–Ag) alloys. Acta Mater 2010;58:5714–23. https://doi.org/10.1016/j.actamat.2010.06.046.
[53] Zindal A, Jain J, Prasad R, Singh SS, Sarvesha R, Cizek P, et al. Effect of heat treatment variables on the formation of precipitate free zones (PFZs) in Mg-8Al-0.5Zn alloy. Mater Char 2018;136:175–82. https://doi.org/10.1016/j.matchar.2017.12.018.
[54] Ogura T, Hirosawa S, Sato T. Quantitative characterization of precipitate free zones in Al–Zn–Mg(–Ag) alloys by microchemical analysis and nanoindentation measurement. Sci Technol Adv Mater 2004;5:491–6. https://doi.org/10.1016/j.stam.2004.02.007.
[55] Embury JD, Nicholson RB. The nucleation of precipitates: the system Al-Zn-Mg. Acta Metall 1965;13:403–17. https://doi.org/10.1016/0001-6160(65)90067-2.
[56] Zhao H, De Geuser F, Kwiatkowski da Silva A, Szczepaniak A, Gault B, Ponge D, et al. Segregation assisted grain boundary precipitation in a model Al-Zn-Mg-Cu alloy. Acta Mater 2018;156:318–29. https://doi.org/10.1016/j.actamat.2018.07.003.
[57] Raghavan M. Microanalysis of precipitate free zones (PFZ) in Al-Zn-Mg and Cu-Ni-Nb alloys. Metall Trans A 1980;11:993–9. https://doi.org/10.1007/BF02654713.
[58] Zhu S, Shih H-C, Cui X, Yu C-Y, Ringer SP. Design of solute clustering during thermomechanical processing of AA6016 Al–Mg–Si alloy. Acta Mater 2021;203:116455. https://doi.org/10.1016/j.actamat.2020.10.074.
[59] Madanat M, Liu M, Zhang X, Guo Q, Čížek J, Banhart J. Co-evolution of vacancies and solute clusters during artificial ageing of Al-Mg-Si alloys. Phys Rev Materials 2020;4:063608. https://doi.org/10.1103/PhysRevMaterials.4.063608.